Journal of Applied Fluid Mechanics, Vol. 11, No. 4, pp. 1073-1088, 2018.
Available online at www.jafmonline.net, ISSN 1735-3572, EISSN 1735-3645.
DOI: 10.29252/jafm.11.04.27632

Systematic Investigation of Thrust Production during Plunging Motion of the Airfoil

H. R. Hamdani[1†] and H. Zareen[2]

[1] *College of Aeronautical Engineering, National University of Sciences and Technology, Islamabad, Pakistan*
[2.] *College of Electrical and Mechanical Engineering, National University of Sciences and Technology, Islamabad, Pakistan*

†*Corresponding Author Email: hossein.hamdani@yahoo.com*

(Received January 26, 2017; accepted January 28, 2018)

ABSTRACT

The effect of various conditions on the thrust generation of 2-D airfoil in pure plunging motion has been investigated. These conditions include different airfoil shapes, different Reynolds numbers (Re) and reduced frequencies (K). The three different shapes used in this study are the NACA0014, the ellipse, and the flat plate airfoil, whereas, the three Re used in the study are 1000, 10000, and 25000 for the three values of K at 2.0, 1.0, and 0.5. For all these parametric studies, the thickness (t/c ratio) of all the airfoil has been kept as constant at 14% t/c ratio. During sinusoidal plunging motion, CL and CD varies in a sinusoidal manner however CL and CD lags with the airfoil motion and the time averaged lift coefficient over one complete cycle is zero whereas the time averaged drag coefficient is negative and non-zero i.e. thrust is produced. The reason behind the thrust generation is due to the formation of the Reverse Karman Vortex Street in the wake of the airfoil.NACA0014 airfoil produces more negative values of the drag coefficient as compared to the ellipse and flat plate which indicates that the shape effect is important for thrust generation which is due to the pressure changes that occur close to the leading edge of the airfoil and it is more pronounced for an airfoil with large Δy variation near the leading edge , for instance NACA 0014. As the Re is increased, the time averaged drag coefficient becomes more negative and the thrust produced by the NACA0014 airfoil remains higher as compared to the other two airfoil which shows that the airfoil shape effect is dominant. As K reduces, time averaged drag coefficient (thrust) decreases and the airfoil shape effect becomes less prominent as K is decreased (or the unsteady effect decreases). It is seen that for all the cases, the CDv (drag due to viscous forces) is very small and major contribution of negative drag (thrust) comes from the pressure forces.

Keywords: Thrust; Reverse Vortex shedding; Airfoil, Vorticity; Plunge; Reduced frequency.

NOMENCLATURE

St	Strouhal number	*K*	reduced frequency
C_p	pressure coefficient	*Re*	Reynolds number
C_L	lift coefficient	*h*	dimensionless stroke amplitude
C_D	drag coefficient	ω	angular frequency
c	chord length	*UDF*	User Defined Function
t	flow time	τ_ω	shear forces acting tangential to the surface of the airfoil
p	pressure forces acting normal to the surface of the airfoil		

1. INTRODUCTION

Micro Air Vehicles (MAV) can be employed for many commercial applications like aerial surveillance, land surveys, as well as for sensing purposes. The design of a Flapping Wing Micro Air Vehicle (FWMAV) is an emerging area of current research especially, the problem of optimal force generation of the flapping wing of an MAV is quite a challenging one. The solution to this problem is particularly helpful for the design and development of MAVs where the optimized lift and thrust

generation is of prime importance.

Most of the early research has been carried out to study the effect of Re and different flapping parameters such as the flapping amplitude, the reduced frequency (‘*K*’ *is non-dimensional frequency, defined later*) and the Strouhal number (*St*) on the aerodynamic performance. Later, the studies have been conducted to see the effect of the geometry of an airfoil on the thrust generation. Tuncer and Platzer (2000) has computed the unsteady, viscous low speed flow over the NACA0012 airfoil in a plunging / pitching motion at various reduced frequencies, amplitudes and phase shifts. They concluded that a high thrust can be obtained when the airfoil is made to plunge at higher frequencies in the presence of large leading edge vortices but the propulsive efficiency becomes significantly low. However, in the case of a combined pitch and plunge motion, the high propulsive efficiency along with the high thrust production can be obtained because the flow remains attached to the airfoil. Ashraf *et al*. (2007) reviewed the progress of the flapping wing aerodynamics and analyzed the effect of the amplitude, the reduced frequencies and the non-dimensional flapping velocity on the thrust generation and the efficiency of a NACA0012 airfoil undergoing pure plunging motion at Re 20000. The results agreed very well with the published data of Heathcote (2006). They also found that some very high values of thrust coefficient but with very low values of efficiency, are generated at the reduced flapping frequency of 2.0 and the non-dimensional plunge amplitude of 24. Young and Lai (2004) numerically investigated the effect of the amplitude and the flapping frequency on the wake of the plunging airfoil. Their study revealed that these computed wake structures are found to be in close agreement with those obtained in the experiments. They concluded that the wake produced by the plunging airfoil strongly depends on both the *K* and the *St* at the given Re. Benkherouf *et al*. (2011) investigated the effect of flapping frequency on the flow physics of the self-propelled flapping airfoil and concluded that the propulsion velocity increases with both the flapping frequency and the amplitude.

The research on the aerodynamic performance of the flapping airfoil has been carried out by using different shapes of the airfoil including the flat plate, the ellipse and the NACA airfoil series. Garrick (1936) investigated the thrust generation and the propulsive efficiency of an oscillating flat plate as a function of the reduced frequency and the non-dimensional flapping velocity. Knowles *et al.* (2007), Sane and Dickinson (2007), Wang et al. (2004) have also employed the flat plate airfoil to study the unsteady aerodynamic behavior of the flapping airfoil by varying different flapping parameters and the flapping kinematics. Wei Shyy (2008) used surrogate modeling to investigate the aerodynamics of hovering elliptic airfoils. Wang (2000) focused on frequency selection in flapping forward flight by using elliptic cross section. A lot of work was carried out on flapping foils by using 4 digit NACA series airfoils. Young and Lai (2007) explained the strong dependence of thrust generation of plunging airfoils on Strouhal number (*St*) and reduced frequency (*K*). Zhao and Yang (2010) investigated the effect of airfoil thickness on flapping performance by using series of NACA airfoils and concluded that with the increase of thickness of airfoil, thrust and propulsive efficiency increases without significant decrease in lift. Ashraf and Lai (2011) also examined the effect of airfoil thickness in plunging and combination of pitching and plunging motion by using NACA airfoils at various Reynolds number. They concluded that thin airfoils outperformed thick airfoils at low Reynolds number due to positive thrust generation. At high Reynolds number, thrust and propulsive efficiency increases with the increase of thickness of the airfoil. They also found the negligible effect on thrust generation by varying the camber location of NACA airfoils. Wen and Liu (2011) studied the mechanism of thrust generation for viscous flow past airfoils in plunging motion by discussing the contribution of pressure and viscous forces. Computations were carried out by varying thickness of elliptic airfoils and also for different shapes of airfoils. They observed that for ellipse having 1% thickness, viscous forces are responsible for thrust generation whereas pressure forces can be ignored from Reynolds number 50-5000. Flow was also simulated on different shapes of airfoils having same thickness at Reynolds number of 100. NACA0012, elliptic and reverse NACA0012 were considered. The results showed that NACA0012 produces greater amount of thrust as compared to other two airfoils.

The published literature shows that most of the studies related to geometry of the airfoil were carried out by varying the thickness of same type of airfoil. This change in the thickness of the airfoil results in change of geometry of the airfoil which affects the aerodynamic force coefficient that is thrust coefficient of the airfoil. A very few studies were carried out to compare the performance of different shapes of airfoil. In addition, studies were also conducted to see the effect of variation of reduced frequency and Reynolds number independently on the thrust generation of the airfoil in pure plunging motion. However, correlation of the effect of airfoil shape, reduced frequency and Reynolds number on thrust generation has not been explored enough.

Present study explores the effect of airfoil shape, Reynolds number and reduced frequency on thrust generation of plunging airfoil. Thrust generation of different shapes of airfoils is investigated at various Reynolds numbers that covers the entire spectrum from fully laminar to fully turbulent regime and then by varying the flapping frequency at the given Reynolds number in order to have the real insight of the variation in the lift and thrust coefficient due to change in airfoil geometry and to explore the correlation of the change of geometry of airfoil with the Reynolds number and flapping frequency of the airfoil. Flapping kinematics is of two types, plunging motion and a combination of pitching and

plunging motion. The purpose of using plunging motion in this study is that various phenomenon of interest of unsteady motion that is thrust generation and Reverse vortex shedding can be obtained with this type of motion.

2. NUMERICAL METHOD

2. 1. Numerical Solver

Unsteady incompressible flow around the plunging airfoil has been computed by solving the 2D Navier Stokes equations in Fluent® using PISO algorithm. A second order upwind scheme is used for the spatial discretization while temporal discretization is limited to a first order accuracy.

2. 2 Computational Grid & Boundary Conditions

The flow field around the airfoil is modeled using a circular domain. The computational domain is discretized using the quadrilateral elements thus forming the structured O-type grid around the airfoil to analyze the flow field as shown in Fig. 1. Since high grid resolution is required near the airfoil surface, therefore, the first grid point is located at a distance of 0.0002c with a wall y^+ value of order 1. A grid close up view is shown in Fig. 2.

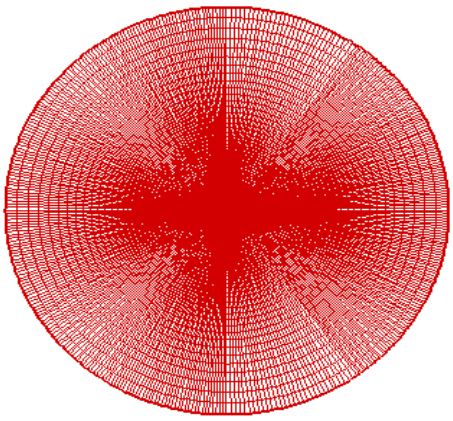

Fig. 1. O – Type grid around the airfoil

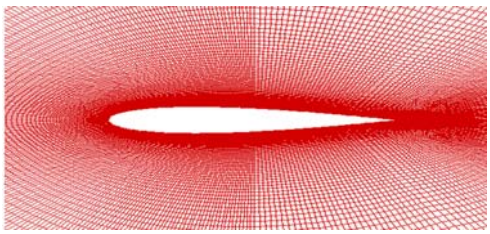

Fig. 2. Grid close up view

This circular domain is divided into two halves where the boundary of one half is defined as the inlet and the boundary of the other half as the outlet. The inlet velocity is used to specify the flow velocity at the inflow and the pressure outlet is used to specify the static pressure at the outflow. A no-slip boundary condition is prescribed on the airfoil surface.

2. 3. Kinematics

A pure plunging motion of an airfoil is defined by the Eq. (1).

$$y(t) = hc\,Cos(\omega t) \tag{1}$$

where, y(t) stands for the instantaneous position of an airfoil, h denotes a dimensionless stroke amplitude with respect to the chord length, c denotes the chord length of an airfoil, and ω is the angular frequency. The plunging motion of an airfoil is shown in Fig. 3.

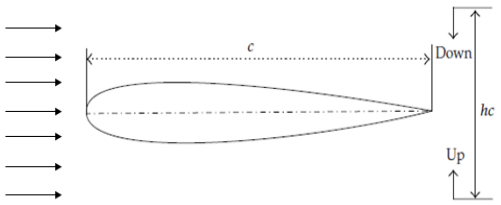

Fig. 3. Plunging motion configuration of an airfoil section

In the present research the motion kinematics of the airfoil is achieved by using dynamic mesh technique employing UDF. The airfoil is treated as a rigid body and the whole mesh moves with the airfoil with the necessary angular velocities at every time step and updates the node positions on the dynamic zones based on the solid body kinematics.

3 VALIDATIONS AND SENSITIVITY STUDIES

In order to check the independence of the numerical solver over the domain and the grid size, the validation studies are carried out by comparing the results with those obtained by Zhao and Yang [15]. The domain independence study is carried out by using two domain sizes of 15c and 20c by keeping the grid size of 401×201 and the time step size of 1e-5. The results obtained are shown in Fig. 4. The plots of lift and drag of both the domain extents are very close to the published results of Zhao and Yang (2010).

Similarly, the grid independence study is carried out by using three grid sizes of 401×201, 401×301 and

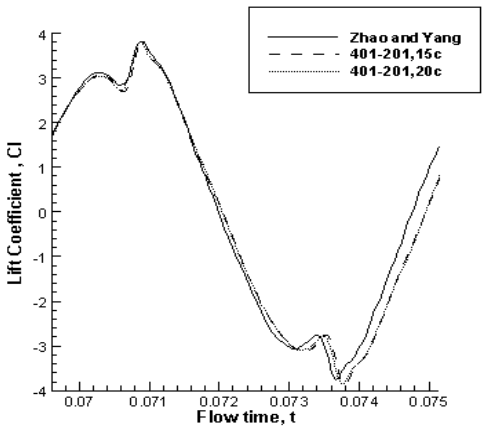

(a) Lift Vs Time Plot

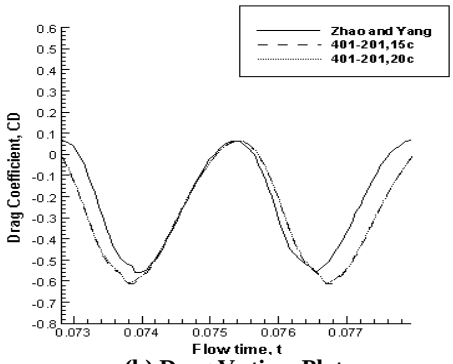

(b) Drag Vs time Plot

Fig. 4. Domain independence study

600×300, respectively. The plots of lift and drag are shown in Fig. 5, indicating that all the three grid sizes have the same values of the force coefficients and are also very near to the published results. Similarly, the time step and the turbulence model sensitivity studies are also carried out in order to choose an appropriate time step size along with the turbulence model.

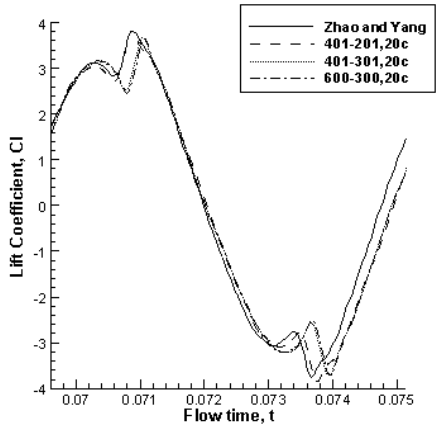

(a) Lift Vs Time Plot

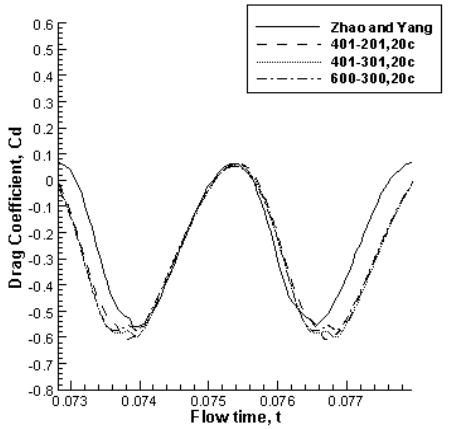

(b) Drag Vs time Plot

Fig. 5. Grid Independence study

The time step sensitivity study is performed by using the two time step sizes of 1e-5 and 3e-5, respectively. The results of both the time step sizes, plotted in Fig. 6, show that the time step size of 1e-5 is giving relatively better approximation of both the lift and drag coefficients with the published results by Zhao and Yang (2010).

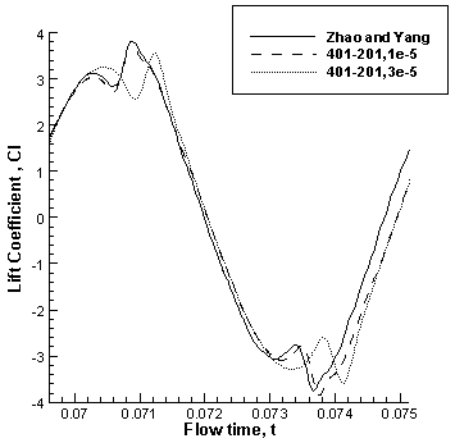

(a) Lift Vs Time Plot

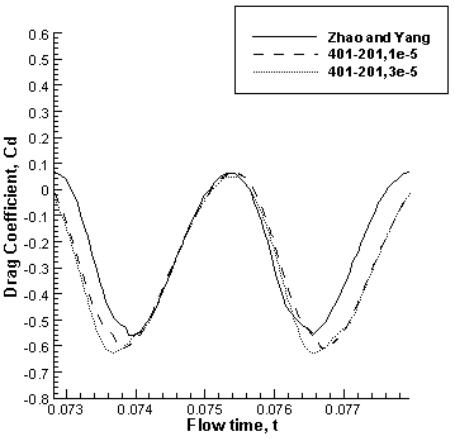

(b) Drag Vs time Plot

Fig. 6. Time step sensitivity

For capturing the turbulence effects at high Re, the turbulence model sensitivity study is also carried out by using S-A and K-ε turbulence models. The lift and drag temporal histories of both the turbulence models are shown in Fig. 7.

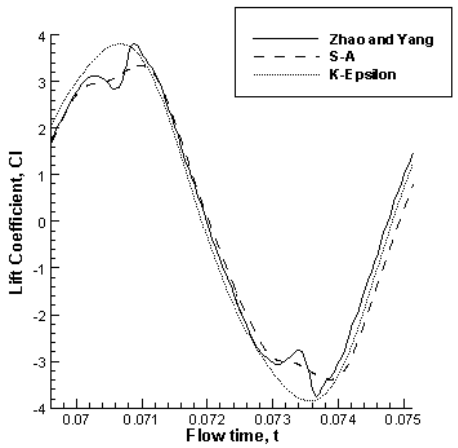

(a) Lift Vs Time Plot

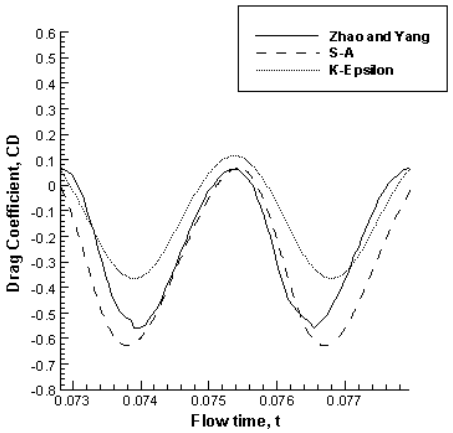

(a) (b) Drag Vs time Plot

Fig. 7. Turbulence model sensitivity study

It is seen from the lift plots, shown in Fig. 7a, that except for slight variations near the upper and lower peak regions, generally the computed values are in good agreement with the published results. On the other hand from the drag plots, the difference in the computed drag plots is slightly more prominent as compared with the published results. However, among the two turbulence models used, the drag plot obtained by using the S-A turbulence model is more close to the published result of Zhao and Yang [15]**.** Also, the drag values are slightly over predicted in S-A turbulence model, possibly due to model induced turbulence effects. Recall, that S-A turbulence model is generally used for the wall bounded flows and has been shown to give good results for the boundary layer problems subjected to the adverse pressure gradients as compared to the K- ε turbulence model. The same trend is observed in the lift and drag plots of both the turbulence models shown in Fig. 7.

Summarizing, domain extent is kept as 15c from airfoil surface and the selected grid size is 401×201. While time step size of 1e-5 is chosen and S-A turbulence model is selected for further computations.

4. RESULTS AND DISCUSSION

4.1. Airfoil Shape Effect

The airfoil shape effect is investigated by using three different shapes of airfoil which include NACA0014, an ellipse and a flat plate at Re 10000 and the reduced frequency K = 2.0. The cross sections of the three airfoil are shown in Fig. 8.

Fig. 8. Cross sections of the three airfoil

The thickness of the three airfoil is kept constant that is 14% of the chord length. Since the validation studies have been performed on NACA0014, its results serve as the baseline and the lift and drag coefficients of the other two cross sections are compared with it. Taking as a guide from the past literature on various shapes of the airfoil used for the MAV applications, these three cross sections have been chosen together in this study for investigating the shape effect. It is pertinent to mention that the previous research deals with these shapes separately to see the effect of various other parameters including the Reynolds number effect, reduced frequency effect, and the thickness effect etc.

The C_L vs. time plot and the C_D vs. time plot are shown in Figs. 9 and 10 respectively. These plots reveal the variation of both C_L and C_D in a sinusoidal behavior, however C_L and C_D lags with the airfoil motion. Figure 9 shows that the C_L vs. time plots for all the three airfoils are identical. It is observed that C_L attains a maximum and a minimum value of approximately +3.5 and -3.5 for the three shapes. However, there is a visible difference in C_D vs. time plots for the three shapes as shown in Fig. 10 i.e. although the drag plots are quite similar in behavior but they do differ in the values as evident from the graph. They do differ in the values as evident from the graph.

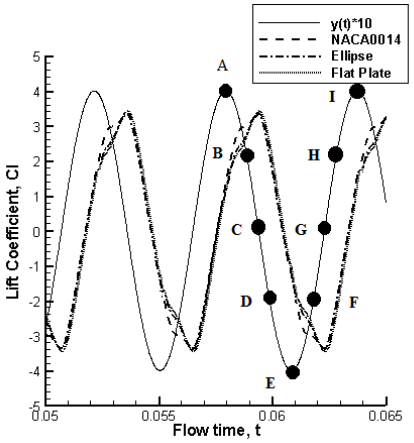

Fig. 9. Lift Vs Time Plot (Re = 10000, *K* = 2.0)

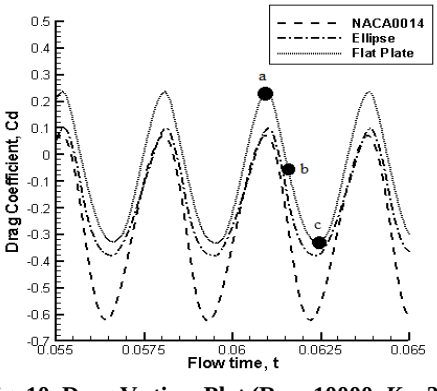

Fig. 10. Drag Vs time Plot (Re = 10000, *K* = 2.0)

From the C_D vs. time plot, the maximum value of C_D for the ellipse is 0.1 and its minimum is -0.31. Similarly, for the flat plate, the maximum and minimum values of C_D are 0.24 and -0.3. For the NACA0014, C_D variation is between 0.08 to -0.61. These values are shown in Table 1. The result from

the Table 1 shows that NACA0014 airfoil produces more negative values of the drag coefficient as compared to the ellipse and flat plate.

Table 1 Instantaneous maximum and minimum values of the lift and drag coefficients

AIRFOIL	Re = 10000, K= 2.0			
	$C_{L\,max}$	$C_{L\,min}$	$C_{D\,max}$	$C_{D\,min}$
NACA0014	+3.5	-3.5	0.08	-0.61
Ellipse	+3.5	-3.5	0.1	-0.31
Flat Plate	+3.5	-3.5	0.24	-0.3

Table 2 represents the time averaged drag and lift coefficients of all the three airfoil. It is observed that the time averaged lift coefficient over one complete cycle is zero whereas the time averaged drag coefficient is negative and non-zero.

Table 2 Time averaged values of the lift and drag coefficients

Airfoil	K = 2.0	
	$\overline{C_L}$	$\overline{C_L}$
NACA0014	0.00	-0.27
Ellipse	0.00	-0.17
Flat Plate	0.00	-0.07

Since the lift vector acts perpendicular to the surface of airfoil, during the down stroke it is pointed upward and during the upstroke it acts in the downward direction. Both the lift vectors cancel each other during a cycle and hence yield zero mean value. However, the drag vector does not change its direction and acts along the surface of the airfoil. During the upstroke and the down stroke, only the alignment of the drag vector is changed. Hence a finite value of the drag is observed. Also, all the three airfoil produce a negative drag i.e. thrust. In order to further investigate this phenomenon, the flow physics of all the cases is explored by plotting the vorticity contours for NACA0014, as shown in Fig. 11.

The vorticity contours have been plotted for the eight points marked on the displacement plot, y(t), during one complete plunge cycle, as shown in Fig. 9. These points are marked alphabetically from A to H. The point A is the start of the down stroke and the airfoil is at the uppermost position. At this position, the vortex is located near the leading edge on the lower side of the airfoil. From the point A to C, this vortex moves downstream and sheds into the wake causing C_L to increase. From point C to D, another vortex forms at leading edge on the upper surface which causes the lift to decrease. And as this vortex moves downstream and sheds (Point E

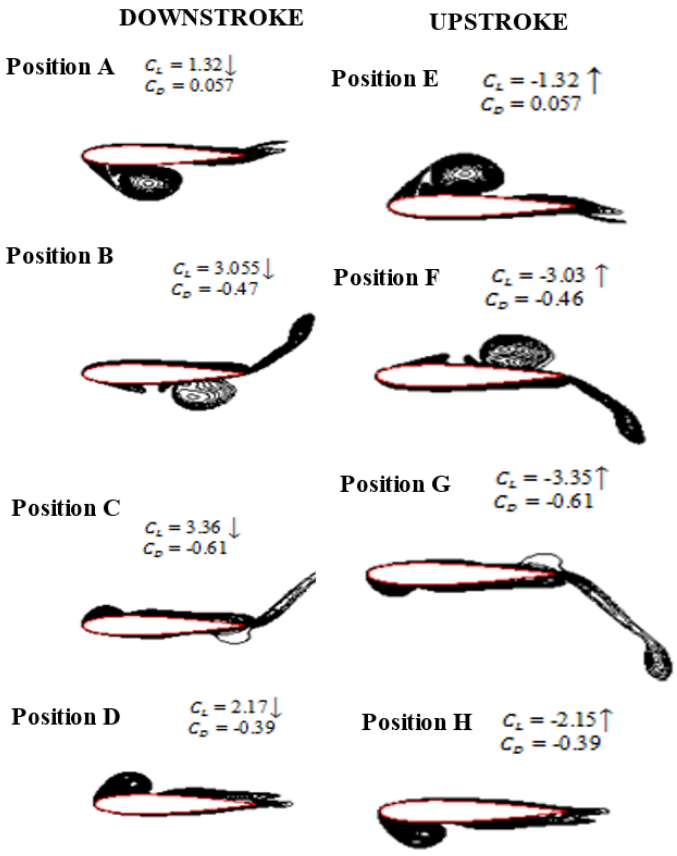

Fig. 11. Vorticity contours of the NACA0014 airfoil

to G), large value of - C_L is generated. This cycle of Reverse Karman Vortex Street repeats with time causing C_L and C_D to have a sinusoidal behavior with time. It is very interesting to note the value of

force coefficients (Fig. 11) during the Upstroke and Downstroke. It is seen that the C_L values are same in magnitude but change sign resulting in net zero lift during a cycle while C_D values do not change the sign during upstroke or downstroke resulting in non zero C_D .

As discussed above, all the shapes of the airfoil produce thrust. The reason behind the thrust generation instead of the drag is due to the formation of the Reverse Karman Vortex Street in the wake of the airfoil. The wake consists of two rows of vortices in which the upper row consists of counter clockwise vortices and the lower row consists of clockwise vortices, as evident from Fig. 11. Now by comparing the vorticity plots of all the three shapes of the airfoil, as shown in Fig. 12, it is seen that the vortex structures are quite similar at all the instants which explains that each airfoil is producing the same amount of lift.

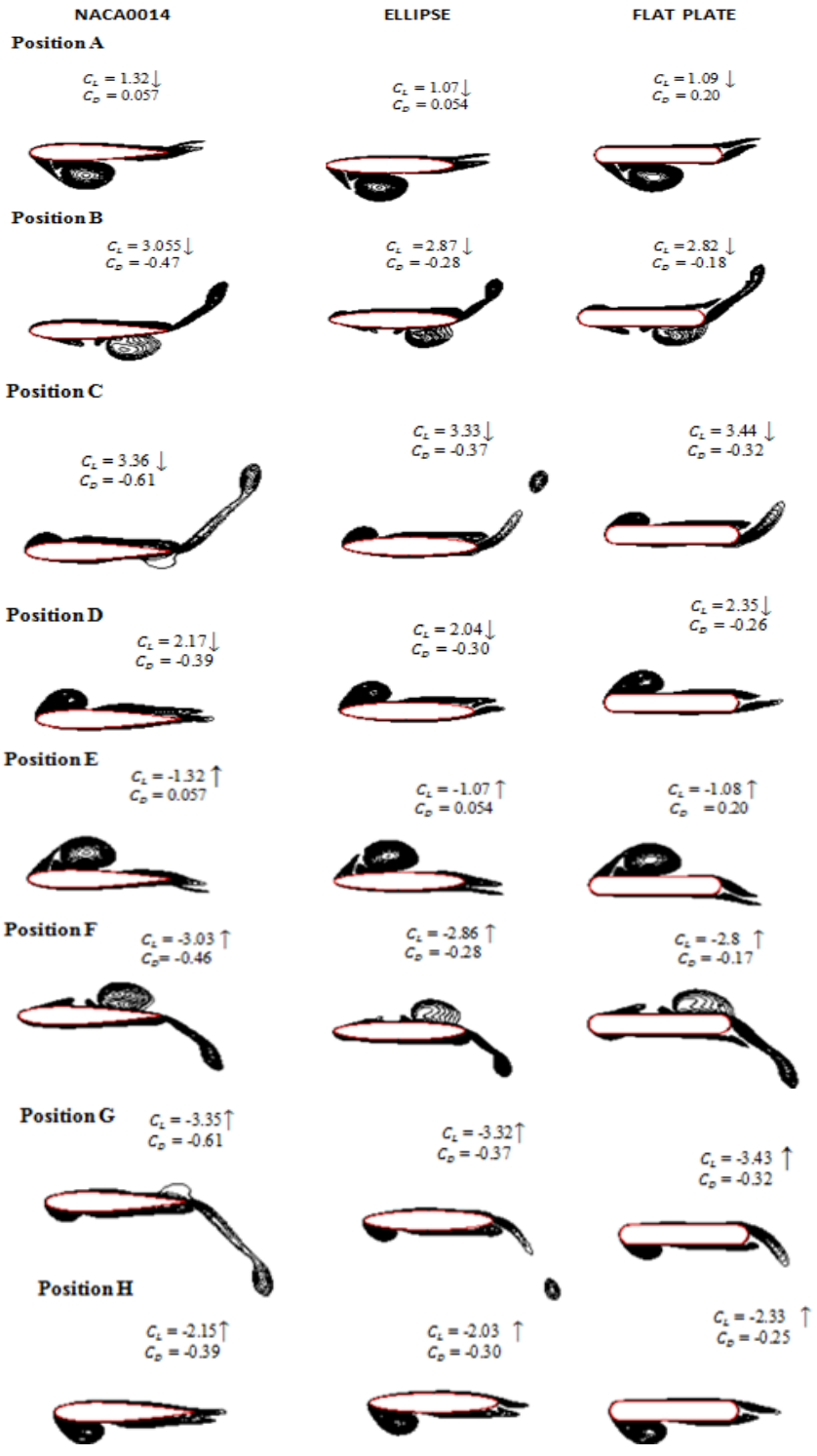

Fig. 12. Vorticity plots of the NACA0014, Ellipse and Flat Plate airfoil

In order to explore thrust production for ellipse and flat plate, both the airfoil are divided into four halves, as shown in Fig. 13. The drag coefficients of the four halves of both the airfoil at maximum, mean and minimum values are then found by calculating the area under the curve of the pressure coefficient vs. y data.

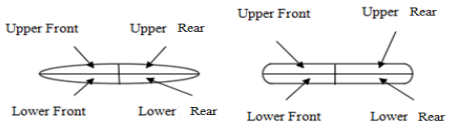

Fig. 13. Four halves of the ellipse and flat plate airfoil

Fig. 14 shows the pressure coefficient plots of the two airfoil at the mean point. Though the vorticity plots are qualitatively similar (Fig. 12), it is seen that the pressure distribution (C_P vs. x) is also similar except at the upper front portion of the airfoil different resulting in different values of C_D ($\overline{C_D}$ for ellipse and flat plate is -0.17 and -0.07 respectively). It is important to note that the curvature at the leading and trailing edge (Fig. 13) of ellipse and flat plate is quite different which causes difference in local flow behavior at these locations. Further it is seen from y vs. C_D plots (Fig. 14 b) that due to the above mentioned curvature effect, the pressure coefficient plots are also different at upper front portion causing difference in drag coefficient. It is known that the drag acting on the small element of the airfoil is given by the Eq. (2).

$$\text{Drag} = D = \int_A (-pdA\sin\theta + \tau_\omega dA\cos\theta) \qquad (2)$$

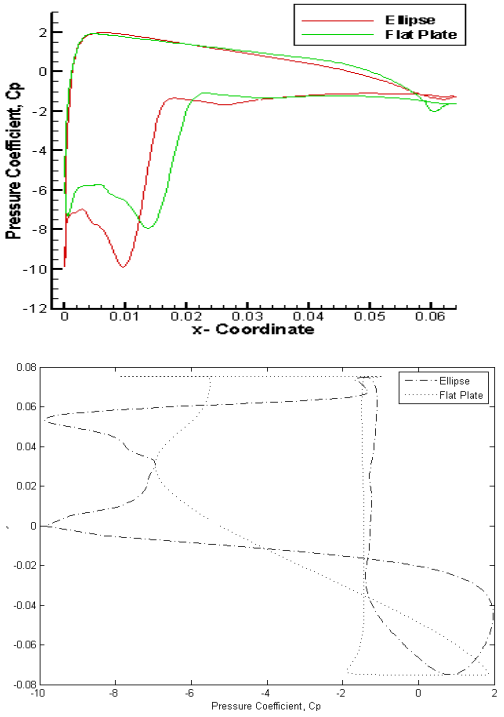

Fig. 14. (a) C_P vs. x and (b) y vs. C_P Plots at Mean point

where, p represents the pressure forces acting normal to the surface of the airfoil and τ_ω represents the shear forces acting tangential to the surface of the airfoil. It will be shown in succeeding paragraphs that the shear force (or viscous force) contribution in overall drag is very less, therefore only pressure force is considered. The pressure forces are multiplied by dAsinθ which actually represents Δy (the height of the element in the vertical direction). For the flat plate, the value of Δy changes only at the leading and trailing edges i.e. from x= 0 to 0.05 and x=0.95 to 1 and for the ellipse, the value of Δy changes uniformly from leading to trailing edge. For NACA0014, the Δy has greater value from leading edge to approximately quarter chord (curvature effect) and from there on till trailing edge, Δy variation is small in comparison with the leading edge portion. According to the earlier discussion, vortical structures (and chord wise pressure distribution) are similar for the three shapes except local flow changes near the leading & trailing edge causing changes in the pressure distribution as seen in Fig. 14a. The effect of these pressure changes in drag contribution is proportional to Δy variation (Eq. (2)) and an airfoil with more Δy variation will be producing more thrust, which is the case for NACA 0014 airfoil.

Table 3 Drag Coefficients of four halves of the airfoil

Airfoil	Maximum Point		Mean Point		Minimum Point	
	Ellipse	Flat Plate	Ellipse	Flat Plate	Ellipse	Flat Plate
Upper Front	0.0385	0.0795	-0.2489	-0.065	-0.4072	-0.3835
Upper Rear	-0.0414	-0.0431	-0.0232	-0.0339	-0.0162	0.0226
Lower Front	0.1523	0.1848	-0.0183	0.107	-0.0712	-0.1661
Lower Rear	-0.0721	-0.0086	0.1121	0.076	0.1292	0.1775
C_D (Calculated)	0.0773	0.2126	-0.1783	0.0841	-0.3654	-0.3455

Table 3 represents the contribution of the four halves of both the airfoil in the total drag coefficient. It is seen that at maximum C_D, lower front portion of the airfoils produce significant drag and at mean C_D and minimum C_D, upper front portion produces thrust and lower rear produces drag.

The vorticity contours have also been plotted for the three points, as shown in Fig. 15 for finding a correlation with pressure plots (Fig. 14 and Table

3). Consistent with the findings from Table 3, at maximum C_D (Fig. 15a), positive vorticity at lower front is responsible for major drag production. At mean C_D (Fig. 15b), positive vorticity has travelled to lower rear portion causing drag production while production of negative vorticity layer at upper front results in thrust production. At minimum C_D (Fig. 15c), positive vorticity is being shed at lower rear portion causing large drag production while strong negative vorticity layer at upper front results in significant thrust production.

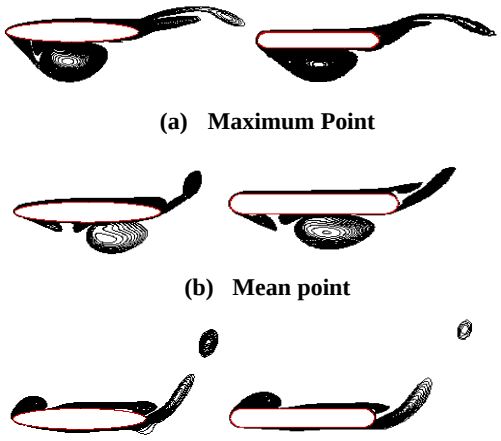

(a) Maximum Point

(b) Mean point

(c) Minimum Point

Fig. 15. Vorticity Contours

Pressure and viscous force contribution at the point of minimum value of the drag coefficient is shown in Table 4.

Table 4 Pressure and viscous force contribution

AIRFOIL	Re = 10,000, K= 2.0			
	C_{Dp}	C_{Dv}	C_D	C_{Dv}/C_D
NACA0014	-0.60	-0.016	-0.62	2.5%
Ellipse	-0.37	-0.005	-0.37	1.3%
Flat Plate	-0.34	0.009	-0.33	2.7%

***C_{Dp}**: Drag coefficient due to pressure forces & **C_{Dv}**: Drag coefficient due to viscous forces*

It is seen that at Re=10,000 and K=2.0, drag contribution due to viscous forces is very small and major contribution of negative drag (thrust) comes from the pressure forces. Last column in table 4 depicts the percentage of viscous forces contribution and it is seen that it is quite small.

4. 2. Reynolds Number Effect

The effect of Re is explored by using its three different values i.e. 1000, 10000, and 25000 respectively. These values of the Re lie in the range for MAVs applications. For investigating the effect of Re, the reduced frequency is kept constant at K = 2.0. The plots of the lift and drag coefficients at the three Re are shown in Figs. 16, 17, and 18 respectively. The lift vs. time plots are quite similar for all the three shapes of the airfoil at all the three values of Re however difference is observed in the drag plots. At Re 1000, the NACA0014 airfoil has more negative values of drag coefficient as compared to the ellipse and flat plate and this difference in the C_D of all the three shapes of airfoil continues to increase with the increase in Re i.e. more thrust is produced as the Re is increased.

The maximum and minimum values of the drag coefficient for all the three cases are given in Table 5. It is seen that the C_{Dmin} becomes more negative as Re increases. Also NACA 0014 produces more thrust than the ellipse and ellipse performs better in thrust production in comparison with the flat plate.

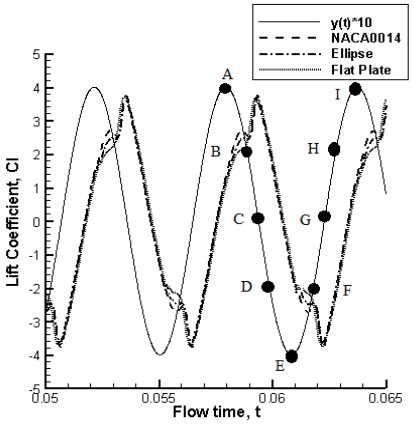

(a) Lift Vs. Time Plot

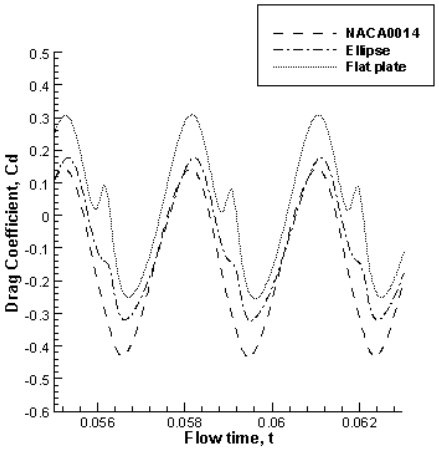

(b) Drag Vs. Time Plot

Fig. 16. (a, & b) Aerodynamic Force Coefficients Plots (Re = 1000, K = 2.0)

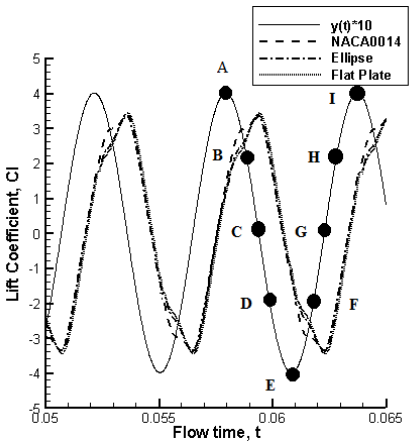

(a) Lift Vs. Time Plot

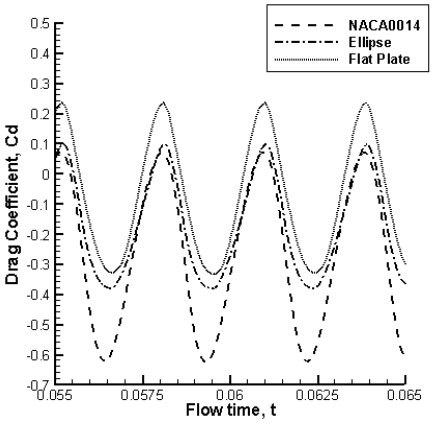

(b) Drag Vs. Time Plot

Fig. 17. (a, & b) Aerodynamic Force Coefficients Plots (Re = 10000, *K* = 2.0)

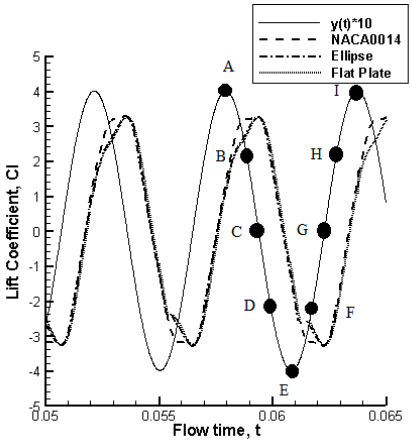

(a) Lift Vs. Time Plot

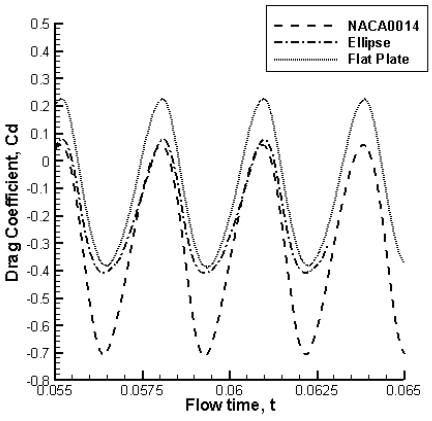

(b) Drag Vs. Time Plot

Fig. 18. (a, & b) Aerodynamic Force Coefficients Plots (Re = 25000, *K* = 2.0)

Table 6 shows the time averaged lift and drag coefficients at all the three Re at the reduced frequency of *K* = 2.0.

The time averaged lift coefficient is seen to be zero at all the three Re, whereas, the time averaged drag coefficient becomes more negative with the increase in Re indicating that the thrust increases with the increase in Re. In order to investigate the reason behind this increase in the thrust generation, the vorticity contours are plotted for NACA0014 airfoil at the three values of Re, as shown in Fig. 19.

It is observed that for the three Re, vortical structure are quite similar except that the vorticity layers around the airfoil surface are more confined at higher Re. Also as Re increases, vorticity gets more confined (for instance Point C and G) and near to the leading edge where the curvature effect (Δy) is large and it results in production of negative drag.

Table 5 Instantaneous maximum and minimum values of drag coefficients

Re	Reduced Frequency, *K* = 2.0					
	NACA0014		Ellipse		Flat Plate	
	C_{Dmax}	C_{Dmin}	C_{Dmax}	C_{Dmin}	C_{Dmax}	C_{Dmin}
1000	0.15	-0.44	0.19	-0.3	0.32	-0.22
10000	0.08	-0.62	0.10	-0.38	0.24	-0.30
25000	0.062	-0.71	0.08	-0.4	0.22	-0.38

Table 6 Time averaged values of lift and drag Coefficients at Re = 1000, 10000 and 25000

Re	Reduced Frequency, *K* = 2.0					
	NACA0014		Ellipse		Flat Plate	
	$\overline{C_L}$	$\overline{C_D}$	$\overline{C_L}$	$\overline{C_D}$	$\overline{C_L}$	$\overline{C_D}$
1000	0.00	- 0.13	0.00	- 0.074	0.00	0.032
10,000	0.00	- 0.27	0.00	- 0.17	0.00	- 0.07
25,000	0.00	- 0.3	0.00	- 0.19	0.00	- 0.10

Pressure and viscous force contribution at the point of minimum drag coefficient for the three airfoil, is presented in Table 7. It is seen that at the three Re and K=2.0, drag contribution due to viscous forces is very small and major contribution of negative drag (thrust) comes from the pressure forces.

Position A

$C_L = 1.26 \downarrow$
$C_D = 0.11$

$C_L = 1.28 \downarrow$
$C_D = 0.041$

$C_L = 1.32 \downarrow$
$C_D = 0.057$

Position B

$C_L = 2.53 \downarrow$
$C_D = -0.21$

$C_L = 3.055 \downarrow$
$C_D = -0.47$

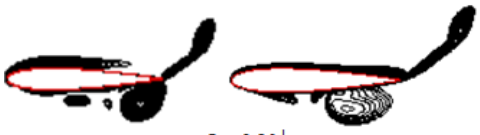

$C_L = 3.20 \downarrow$
$C_D = -0.51$

Position C

$C_L = 3.64 \downarrow$
$C_D = -0.42$

$C_L = 3.36 \downarrow$
$C_D = -0.61$

$C_L = 3.28 \downarrow$
$C_D = -0.69$

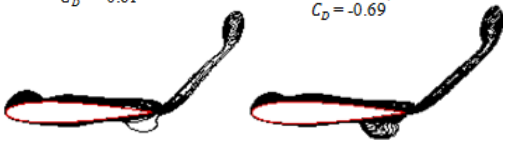

Position D

$C_L = 2.06 \downarrow$
$C_D = -0.29$

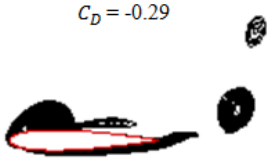

$C_L = 2.17 \downarrow$
$C_D = -0.39$

$C_L = 2.35 \downarrow$
$C_D = -0.44$

Position E

$C_L = -1.26 \uparrow$
$C_D = 0.11$

$C_L = -1.32 \uparrow$
$C_D = 0.057$

$C_L = -1.28 \uparrow$
$C_D = 0.042$

Position F

$C_L = -2.51 \uparrow$
$C_D = -0.21$

$C_L = -3.18 \uparrow$
$C_D = -0.51$

$C_L = -3.03 \uparrow$
$C_D = -0.46$

Position G

$C_L = -3.63 \uparrow$
$C_D = -0.42$

Position H

$C_L = -3.35 \uparrow$
$C_D = -0.61$

$C_L = -3.26 \uparrow$
$C_D = -0.69$

$C_L = -2.04 \uparrow$
$C_D = -0.29$

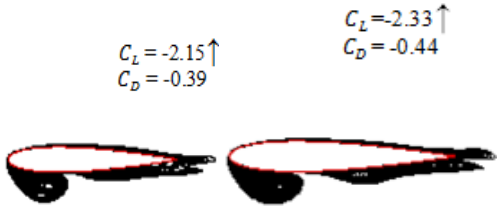

Fig. 19. Vorticity contours at Re = 1000, 10000, and 25000

Table 7 Contribution of pressure and viscous forces at Re = 1000, 10000, and 25000

Re	Reduced frequency, K = 2.0								
	NACA0014			Ellipse			Flat Plate		
	C_{Dp}	C_{Dv}	C_D	C_{Dp}	C_{Dv}	C_D	C_{Dp}	C_{Dv}	C_D
1000	-0.43	0.011	-0.42	-0.31	-0.002	-0.31	-0.28	0.036	-0.25
10000	-0.60	-0.016	-0.62	-0.37	-0.005	-0.37	-0.34	0.009	-0.33
25000	-0.69	-0.013	-0.70	-0.40	-0.007	-0.40	-0.38	0.001	-0.38

From the above discussion, it can be stated that the thrust increases with the increases in Re. The thrust produced by the NACA0014 airfoil remains higher as compared to the other two airfoil at all the Re, which shows that the airfoil shape effect is dominant.

4.3. Reduced Frequency Effect

The reduced frequency ($K=2\pi fc/U_\infty$) is the non-dimensional form of the flapping frequency (f) normalized with the help of the chord length (c) and the free stream velocity (U_∞). It may also be seen as a measure of the unsteadiness. The effect of reduced frequency on the three different airfoil is investigated by using three different values of K = 2.0, 1.0 and 0.5. The corresponding values of the flapping frequency, in Hz, are shown in Table 8.

Table 8 Reduced frequencies and their corresponding values in Hz

Reduced Frequency (K)	Flapping Frequency (Hz)
2	172.5
1	86.2
0.5	43.1

As for the biological flyers, the flapping frequency ranges between 10-600 Hz, whereby the chosen frequencies are within this range showing that the choice of reduced frequencies is suitable for the present study. By keeping the Re 10000 as constant, the aerodynamic force coefficients are plotted for investigating the reduced frequency effect. These plots are shown in Figs. 20, 21, and 22, for each of the three selected K values, respectively.

At K = 2.0, the three airfoil have the similar lift plots while difference is observed in the drag plots of the airfoil. A slight increase in the value of the lift coefficient is also observed for the flat plate as compared to the other two airfoil at K = 1.0 and 0.5, whereas the difference in the drag plots of the three airfoil decreases as compared to K = 2.0. Summarizing it can be said that the airfoil shape effect becomes less dominant as K is decreased (or the unsteady effect decreases).

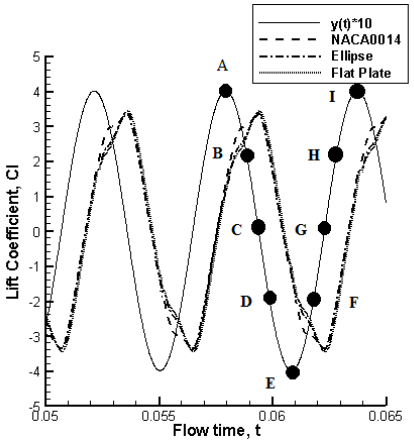

(a) Lift Vs. Time Plot

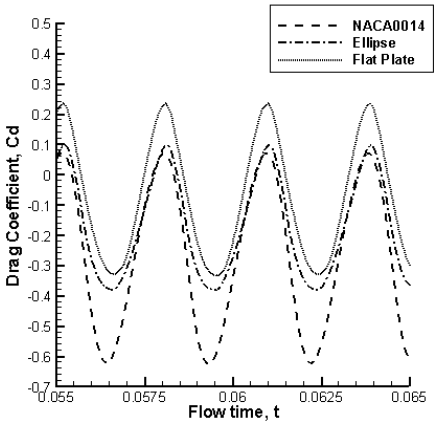

(b) Drag Vs. Time Plot

Fig. 20. (a, & b) Aerodynamic Force Coefficients Plots (Re = 10000, K = 2.0)

Table 9 shows the Time averaged lift and drag Coefficients at reduced frequencies of K = 2.0, 1.0 and 0.5. It is observed that the time averaged lift coefficient is zero for all the three shapes of airfoil. It is seen that as K reduces, time averaged drag

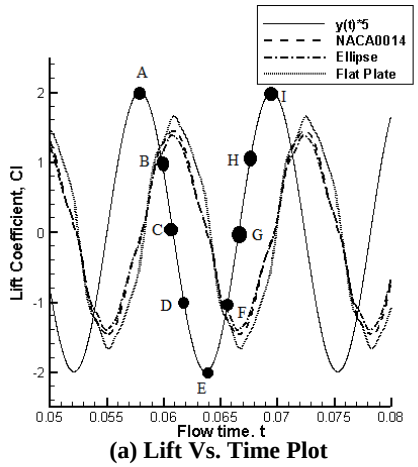

(a) Lift Vs. Time Plot

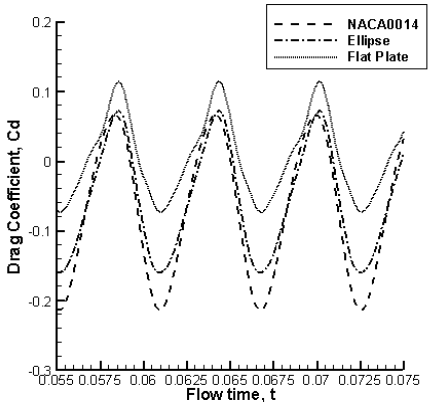

(b) Drag Vs. Time Plot

Fig. 21. (a, & b) Aerodynamic Force Coefficients Plots (Re = 10000, *K* = 1.0)

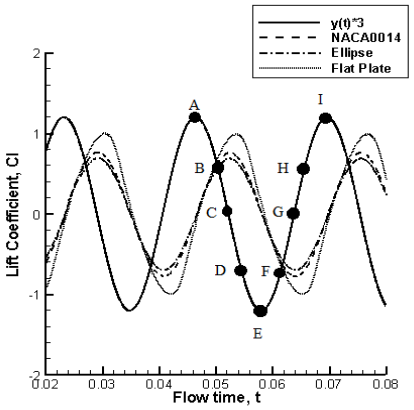

(a) Lift Vs. Time Plot

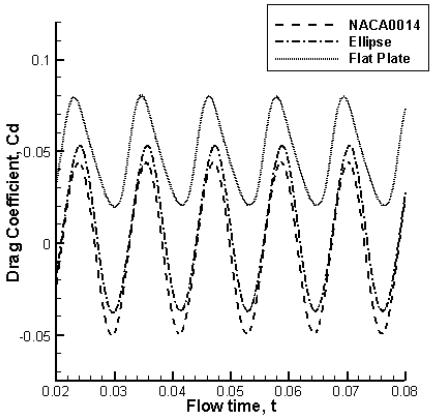

(b) Drag Vs. Time Plot

Fig. 22. (a, & b) Aerodynamic Force Coefficients Plots (Re = 10000, *K* = 0.5)

coefficient (thrust) decreases and at K=0.5, thrust is being no more produced.

Table 9 Time averaged lift and drag Coefficients at reduced frequencies of *K* = 2.0, 1.0 and 0.5

K	Re = 10000					
	NACA0014		Ellipse		Flat Plate	
	$\overline{C_L}$	$\overline{C_D}$	$\overline{C_L}$	$\overline{C_D}$	$\overline{C_L}$	$\overline{C_D}$
2.0	0.00	-0.27	0.00	-0.17	0.00	-0.07
1.0	0.00	-0.067	0.00	-0.05	0.00	0.01
0.5	0.00	-0.002	0.00	0.007	0.00	0.048

The vorticity plots of the NACA0014 at all *K* are shown in Fig. 23 for exploring its effect on the flow physics and the thrust production.

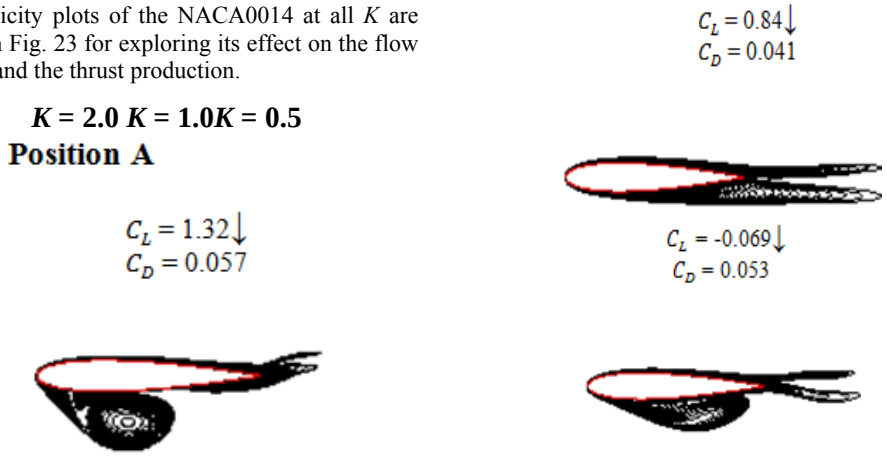

Position B

$C_L = 3.055 \downarrow$
$C_D = -0.47$

$C_L = 1.27 \downarrow$
$C_D = -0.11$

$C_L = 0.63 \downarrow$
$C_D = -0.01$

Position C

$C_L = 3.36 \downarrow$
$C_D = -0.61$

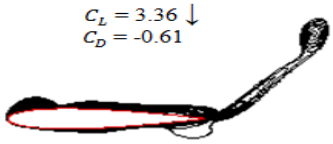

$C_L = 1.44 \downarrow$
$C_D = -0.21$

$C_L = 0.76 \downarrow$
$C_D = -0.04$

Position D

$C_L = 2.17 \downarrow$
$C_D = -0.39$

$C_L = 1.21 \downarrow$
$C_D = -0.15$

$C_L = 0.67 \downarrow$
$C_D = -0.03$

Position E

$C_L = -1.32 \uparrow$
$C_D = 0.057$

$C_L = 0.17 \uparrow$
$C_D = 0.04$

$C_L = 0.06 \uparrow$
$C_D = 0.053$

Position F

$C_L = -3.03 \uparrow$
$C_D = -0.46$

$C_L = -1.27 \uparrow$
$C_D = -0.11$

$C_L = -0.63 \uparrow$
$C_D = -0.01$

Position G

$C_L = -3.35 \uparrow$
$C_D = -0.61$

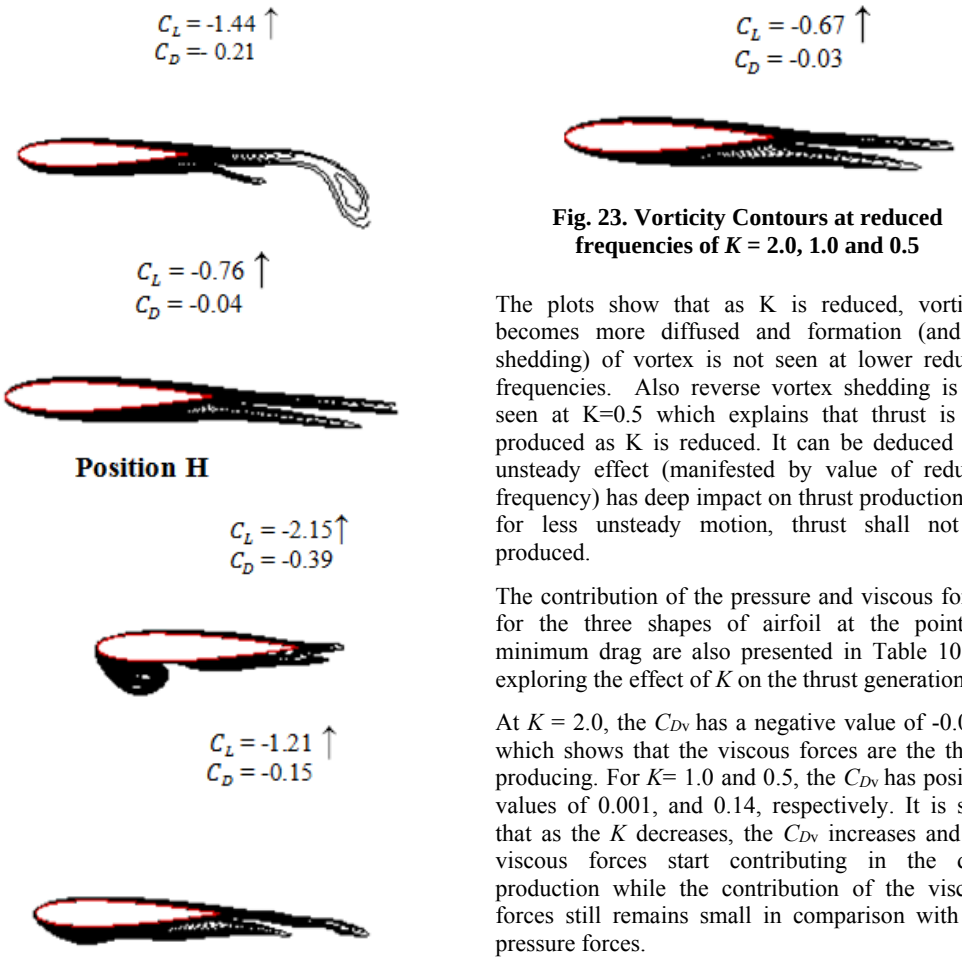

Fig. 23. Vorticity Contours at reduced frequencies of *K* = 2.0, 1.0 and 0.5

The plots show that as K is reduced, vorticity becomes more diffused and formation (and its shedding) of vortex is not seen at lower reduced frequencies. Also reverse vortex shedding is not seen at K=0.5 which explains that thrust is not produced as K is reduced. It can be deduced that unsteady effect (manifested by value of reduced frequency) has deep impact on thrust production i.e. for less unsteady motion, thrust shall not be produced.

The contribution of the pressure and viscous forces for the three shapes of airfoil at the point of minimum drag are also presented in Table 10 for exploring the effect of *K* on the thrust generation.

At *K* = 2.0, the C_{Dv} has a negative value of -0.016, which shows that the viscous forces are the thrust producing. For *K*= 1.0 and 0.5, the C_{Dv} has positive values of 0.001, and 0.14, respectively. It is seen that as the *K* decreases, the C_{Dv} increases and the viscous forces start contributing in the drag production while the contribution of the viscous forces still remains small in comparison with the pressure forces.

Table 10 Contribution of pressure and Viscous coefficients at reduced frequencies *K* = 2.0, 1.0 and 0.5

K	Re = 10000								
	NACA0014			Ellipse			Flat Plate		
	C_{Dp}	C_{Dv}	C_D	C_{Dp}	C_{Dv}	C_D	C_{Dp}	C_{Dv}	C_D
2.0	-0.60	-0.016	-0.62	-0.37	-0.005	-0.37	-0.34	0.009	-0.33
1.0	-0.21	0.001	-0.21	-0.16	0.004	-0.15	-0.08	0.011	-0.07
0.5	-0.063	0.014	-0.049	-0.05	0.016	-0.036	0.008	0.012	0.02

5 CONCLUSION

NACA 0014, Ellipse and Flat plate have been chosen in this study for investigating the effect of airfoil shape on thrust production at different Re and Reduced frequencies. During sinusoidal plunging motion at K=2 and Re=10000, C_L and C_D varies in a sinusoidal manner however C_L and C_D lags with the airfoil motion. It is observed that the time averaged lift coefficient over one complete cycle is zero whereas the time averaged drag coefficient is negative and non-zero i.e. thrust is produced. The reason behind the thrust generation is due to the formation of the Reverse Karman Vortex Street in the wake of the airfoil.NACA0014 airfoil produces more negative values of the drag coefficient as compared to the ellipse and flat plate which indicates that the shape effect is important for thrust generation. This is due to the pressure changes which occur close to the leading edge of the airfoil and it is more pronounced for an airfoil with large Δy variation near the leading edge , for instance NACA 0014. At K=2 and Re=1000, 10000 and 25000; the time averaged lift coefficient is zero whereas the time averaged drag coefficient becomes more negative with the increase in Re indicating that the thrust increases with the increase in Re. The thrust produced by the NACA0014 airfoil remains higher as compared to the other two airfoil at all the Re, which shows that the airfoil shape effect is dominant. Computations were performed at K=2, 1 and 0.5; it is seen that as K reduces, time averaged drag coefficient (thrust) decreases and at K=0.5, thrust is being no more produced and the airfoil shape effect becomes less prominent as *K* is decreased (or the unsteady effect decreases). It is seen that for all the cases, the C_{Dv} (drag due to viscous forces) is very small and major contribution of negative drag (thrust) comes from the pressure forces.

REFERENCES

Ashraf, M. A., J. C. S. Lai and J. Young (2007). Numerical Analysis of Flapping Wing Aerodynamics. *16th Australian Fluid Mechanics Conference,* Crown Plaza, Gold Coast, Australia.

Ashraf, M. A., J. Young, J. C. S. Lai (2011). Reynolds number, thickness and camber effects on flapping airfoil propulsion. *Journal of Fluids and Structures* 27, 145–160.

Benkherouf, T., M. Mekadem, H. Oualli, S. Hanchi, L. Keirsbulck, L. Labraga (2011). Efficiency of an auto-propelled flapping airfoil. *Journal of Fluids and Structures* 27, 552–566.

Garrick, I. E. (1936). Propulsion of a flapping and oscillating airfoil. *NACA Report Number,* 567.

Heathcote, S., Z. Wang, and I. Gursul (2008). Effect of Spanwise Flexibility on Flapping Wing Propulsion. *Journal of fluids and structures* 24(2): 183-199

Ismail H., Tuncer, F. Platzer Max (2000). Computational Study of Flapping Airfoil Aerodynamics. *Journal of Aircraft* 37(3), 514-520.

Knowles, K., Wilkins, P. C., Ansari, S. A., Zbikowski, R. W. (2007). Integrated Computational and Experimental Studies of Flapping-wing Micro Air Vehicle Aerodynamics. *3rd International Symposium on Integrating CFD and Experiments in Aerodynamics*, U. S. Air Force Academy, CO, USA.

Sane, S. P., Dickinson, M. H. (2001). lift and drag. *The Journal of Experimental Biology* 204, 2607–2626.

Trizila, P. and W. Shy (2008). A Surrogate Model Approach in 2D versus 3D Flapping Wing Aerodynamic Analysis. *12th AIAA/ISSMO Multidisciplinary Analysis and Optimization Conference.* Victoria, British Columbia Canada.

Wang, Z. J. (2000). Vortex Shedding and Frequency Selection in Flapping Flight. *Journal of Fluid Mechanics* 410, 323–341.

Wang, Z. J., Birch, J. M., Dickinson M. H. (2004).Unsteady forces and flows in low Reynolds number hovering flight: two-dimensional computations vs. robotic wing experiments. *The Journal of Experimental Biology* 207, 449-460.

Wen, M. H., W. R. Hu, and H. Liu (2011). Thrust Generation Mechanism on Wing Heaving Motion. *AIP Conf. Proc*. 1376, 190-193.

Young, J. and Lai, J. C. S. (2004). Frequency and Amplitude Effects in the Wake of a Plunging Airfoil. *AIAA Journal* 42(10): 2042–2052.

Young, J., C. S. Joseph Lai (2007). On the Aerodynamic Forces of a Plunging Airfoil. *Journal of Mechanical Science and Technology* 21, 1388-1397.

Zhao, L. and S. Yang (2010). Influence of Thickness Variation on the Flapping Performance of Symmetric NACA Airfoils in Plunging Motion. *Hindawi Publishing Corporation*, *Mathematical Problems in Engineering, 675462:19 pages.*